Journal of Materials Chemistry C

Accepted Manuscript

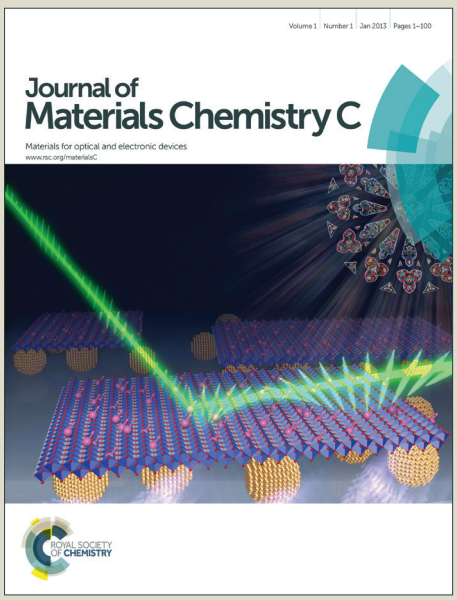

ROYAL SOCIETY OF CHEMISTRY

www.rsc.org/materialsC

ARTICLE TYPE www. rsc.org/xxxxxx | XXXXXXXX

Low-absorption, multi-layered scintillating material for high resolution real-time X-ray beam analysis

Antonio Pereira,[a] Thierry Martin,[b] Mariana Levinta,[a] and Christophe Dujardin*[a]

Received Xth XXXXXXXXXX 20XX, Accepted Xth XXXXXXXXX 20XX
First published on the web Xth XXXXXXXXXX 200X
DOI: 10.1039/b000000x

For on-line X-ray beam analysis, we introduce a functional device, a multilayer scintillating screen, that succeeds in satisfying three important criteria: high X-ray transparency and high overall efficiency, which are not easily reconcilable with existing devices, as well as high spatial resolution capability. It combines a porous alumina substrate, an optical gold interposer of few nm and an efficient scintillating material (Lu_2O_3:Eu^{3+}) 450 nm thick. Both layers are deposited using pulsed laser deposition. This multilayer device enables high resolution X-ray images while X-ray transparency is preserved to 90% even at 15 keV. Such a device is suitable for real-time X-ray beam analysis at high frequency and is a breakthrough for real-time X-ray beam corrections for most of the synchrotron experiments

1 Introduction

Synchrotron radiation facilities offer all around the world a unique tool for X-ray analysis of matter. From life science to atomic, molecular and material sciences, the produced X-ray beam enables a deep understanding in many fields of sciences such as physics, chemistry, biology and even medicine. All the experiments are based on the physical response of a sample to a monochromatic coherent X-ray beam, eventually with time-resolved properties. Technically, scientists collect X-ray images, diffracted beam, photo-electrons or emission of light during their measurements. All these techniques are nowadays pushed toward their limits in order to improve matter exploration. As illustrations, 60 nm X-ray image resolution can be achieved in a tomography regime or time resolved X-ray diffraction on nano-domains.[1,2] One of the major limitations for the improvement in performance is due to the incident X-ray beam fluctuations in terms of position, intensity and shape. Current technologies of X-ray beam analysis do not allow online measurement of the whole beam characteristics simultaneously with the experiment, which is a crucial issue to achieve a breakthrough on the performances. They use either photocurrent or scintillation induced by interaction of the X-ray beam with a sensor or convertor. In addition, in order to preserve the experiment acquisition time, the beam sensor has to preserve the incident X-ray beam, and the X-ray absorption has to be limited to 10%, which is a critical issue, mainly at low X-ray energies. Combining weak X-ray absorption and precise informations collected a short time is challenging since these two criteria are contradictory. In this paper, we report the preparation, characterization and achieved performances of a scintillator-based multilayered device. We demonstrate its ability to be used as online beam position, shape and intensity monitors on all X-ray synchrotron beamlines with monochromatic energy over 15 keV. Previous works based on a converter screen or pin-hole camera have demonstrated the attractiveness of 2D image (shape, position and intensity of X-ray beam) but they were limited in terms of 12 μm spatial resolution and 400 nm position resolution respectively.[3,4] In the energy range 5-30 keV, single crystal diamond with four metalized electrodes operated as a solid state ionization chamber reaches down to 20 nm precision position but does not provide shape or 2D information.[5] The method based on a 2D image provided by a thin and dense converter film allows high beam position precision (below 100 nm) and high imaging resolution (1-10 μm spatial resolution) to be reached.

2 Experimental section

2.1 Synthesis of scintillating structures

Gold and Lu_2O_3:Eu^{3+} were deposited onto commercially 60 μm thick AAO membranes (Anodisc13, Whatman) consisting of an ordered array of holes (100 nm in diameter) by Pulsed Laser Deposition (PLD) at room temperature. A pure polycrystalline Au target (99.99%, Kurt J. Lesker Co.) and a Lu_2O_3:1%Eu^{3+} target were ablated by means of a pulsed KrF excimer laser (λ = 248 nm, pulse width = 17 ns, and repetition rate = 10 Hz) in a high vacuum deposition chamber (residual

[a] *Institut Lumière Matière, UMR5306 Université Lyon1 CNRS, Université de Lyon, 10 rue Ada Byron, Villeurbanne 69622, France, Fax: (33) 472 43 11 30; Tel:(33) 472 44 83 36; E-mail: christophe.dujardin@univ-lyon1.fr*
[b] *ESRF-The European Synchrotron, 71 avenue des Martyrs, 38000 Grenoble, France*

pressure of 2x10^{-7} mbar). Eu^{3+} doped Lu_2O_3 was previously synthetized by solid state reaction (6 h at 1400 °C in air), after grinding and mixing Lu_2O_3 (99.99% purity, Alfa Aesar) and Eu_2O_3 (99.99% purity, Alfa Aesar). For all experiments, the laser fluence was kept constant at 4 J/cm^2. Lu_2O_3:Eu^{3+} films were deposited under 10^{-3} mbar of oxygen and the target-to-substrate-distance ($d_{t\text{-}s}$) was set to 4 cm. For each material and deposition conditions, the deposition rate was first determined by profilometric measurements. The number of laser pulses was then adjusted to achieve 450 nm of Lu_2O_3:Eu^{3+} and 20 nm of Au. The layer onto layer Lu_2O_3:Eu^{3+} / Au nanostructures were deposited by alternating the ablation of the two targets without breaking the vacuum. A rapid thermal annealing (Jipelec JetFirst furnace) of the deposited multilayers was then realized at 450 °C in air for 10 s.

2.2 Characterization

The crystallization state of Lu_2O_3 was characterized by X-ray diffraction (XRD) using a Rigaku SmartLab diffractometer with a Cu Kα radiation in the Bragg-Brentano θ - 2θ configuration. The morphology was investigated by scanning electron microscopy (SEM, Hitachi S800 FEG). Luminescence spectra have been recorded under 250 nm excitation coming out of a 450 W Xenon lamp coupled with a double monochromator Gemini from Jobin Yvon. The emission light has been collected through an optical fiber coupled to a Triax 320 from Jobin Yvon equipped with a CCD camera 3000. X-ray characterizations were performed at the ESRF on the beamline BM05. This beamline delivers white or monochromatic beams, and offers a large energy range from 6 keV to 60 keV as well as the choice between two monochromators: Δ/E$<10^{-4}$ with Si(111) crystals and ΔE/E$<10^{-2}$ with multilayers. A Kirkpatrick-Baez (KB) mirror system has been used for the focus beam application. The device produces X-ray beam down to $\sim$2.5 x 1.5 μm (horizontal x vertical). Objects and micro-charts have been imaged with X-ray provided by the multilayer monochromator. The detector consists of a charged-couple device (Basler camera Aca 1300gm), an optics (1x or 2x magnification) and in-house mechanics. Images have been corrected by the flat field and dark current. The X-ray attenuation has been measured with the Si(111) monochromator and a Canberra photodiode placed sequentially upstream and downstream the sample to analyze.

3 Results and discussion

3.1 Performance requirements and multilayer approach

Because the final application has to satisfy many performance types, the scintillator selection and shape are the result of a compromise between various quality criteria. The device has to combine good X-ray transparency and high-resolution imaging capability. Limiting the X-ray absorption to a few percent is rather contradictory to the detection efficiency and to the scintillation principle, which requires as many of absorbed X-ray photons as possible. Nevertheless, in the particular case of synchrotron radiation facilities, the X-ray beam flux is so high (typically 10^{13}-10^{14} ph/s/mm^2 for modern beamlines) that even a weak X-ray absorption in the order of few percent combined with a scintillator exhibiting a high scintillation yield is acceptable. The intensity of emitted light is in this case sufficient to extract a significant optical signal for beam analysis. Since high-resolution images are obtained using refractive lenses combined with a camera, the scintillating image emerging from the scintillator has to remain in the focus depth of the objective. It has been shown in the frame of high resolution X-ray imaging that thicknesses in the order of 1 to 5 micrometers are ideal to achieve the best imaging resolution.[6] With such a small thickness, traditional cutting and polishing from bulk materials are not appropriate, and a layer deposition technique is required. Nevertheless, this technique requires a substrate for mechanical hardness of the device and easy handling, which is a drawback regarding X-ray transparency. Considering the small required area (2x2 cm), Pulsed Laser Deposition is suitable since it has been proved to deposit, with good optical quality, almost all kinds of oxides as a crystalline phase, which is consistent with most of the traditional scintillator compositions.[7–9] In our case we selected the binary compound Lu_2O_3 activated with the Eu^{3+} ion. We could have chosen another scintillators such as cerium doped garnet if one looks only at scintillating performance, but the optical quality is also critical when high resolution imaging is desired, and it requires thus a good control of the synthesis. With Pulsed laser deposition, ternary compounds are much more complicated to obtain. Indeed, PLD decomposes the target and leads to a plasma plume which evolves in a out-of-equilibrium process. In case of a garnet such as $Lu_3Al_5O_{12}$ (LuAG), the resulting film is produced by the physico-chemical reaction in the plasma plume which can lead to the LuAG phase, but also to other phases such as Al_2O_3, Lu_2O_3 and potentially the perovskite phase, able to deteriorate the optical quality. The selected binary Eu^{3+} doped compound Lu_2O_3 is a scintillating material and its analog Gd_2O_3 have already been prepared as powders, ceramics and thin films via chemical vapor deposition, sol-gel dip-coating techniques and Pulsed Laser Deposition. It is well known to exhibit a scintillation yield of about 20000 photons / Mev in the X-ray range and a weak afterglow which is crucial in case of fast imaging.[10–17] In addition, its spectral properties, i.e. a red emission peaking at 610 nm, is well adapted to the efficiency of most of the CCD cameras. Selection of the substrate is a critical issue since it has to preserve the X-ray transparency and has to be adapted for oxide deposition in terms of surface treatments. We selected com-

mercial filters based on porous alumina. Such substrates have a low cost, a rather weak density and the porosity favors the weak X-ray absorption. We calculate with the NIST database the theoretical X-ray attenuation as a function of the energy for a thickness of 60 μm which corresponds to commercial anodic alumina oxide (AAO) membrane (Fig.1, red line for theoretical and full circle for measurements). We measured the X-ray transmission of these membranes, and the result is in good agreement with alumina having a filling factor of 33%. These results show that transmission below 12% is preserved for X-ray energy down to 12 keV which satisfies the high transmission requirement. Note that 450 nm thick Lu_2O_3 layer (Fig. 1, blue line) and the substrate contribute about equally to the X-ray beam attenuation in this energy range. If the porosity is favorable to decrease the X-ray absorption, it also deteriorates the optical quality of the substrate inducing a potential blurring of the reflected image from the scintillator. We thus propose to compare a Lu_2O_3/AAO structure and a structure containing an intermediate layer of gold (few tens of nanometers thick) aiming either to optically isolate the scintillator from the porous material and/or to smooth the substrate surface. Regarding X-ray attenuation, Fig. 1 shows that a 20 nm thick gold film has a negligible (<1%) contribution to the X-ray attenuation in this energy range (Fig. 1, green line) while its optical transparency is already weak. The comparison is performed in terms of imaging capability which is quantified via the Modulation Transfer Function (MTF).

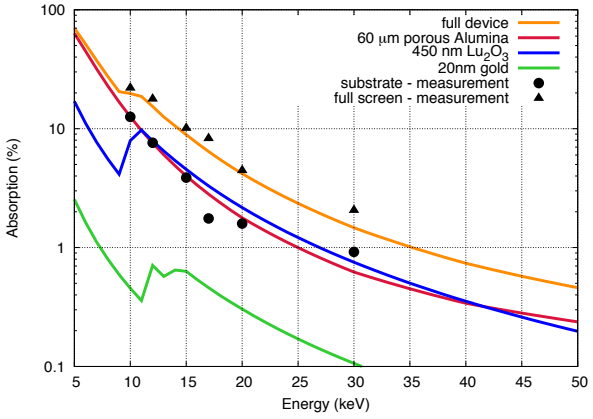

Fig. 1 Solid colored lines - theoretical attenuation for dots: 20 nm of gold (green), 450 nm of Lu_2O_3 (blue), 60 μm of porous (33%) alumina (red) and the combination of these 3 components representing our screen (orange). Measurement of the free membrane used as a substrate (full circles) and of the full screen (full triangles)

3.2 Device preparation and characterization

The multilayer structures constituted of an Au layer covered by a Lu_2O_3:Eu^{3+} scintillating layer were deposited on AAO membranes by using PLD. Technical details are reported in the experimental section below. Regarding the gold optical interposer, two preparation conditions have been tested to improve the imaging capability of the scintillating screen. In a previous work, we reported the deposition of metallic films on AAO membranes.[18] Various morphologies of Pt, Au and Pt-Ru films were obtained by controlling the kinetic energy of the ablated species. At high kinetic energy, i.e under vacuum or moderate pressures, the nucleation and growth of particles on a substrate are dominated by surface diffusion processes. Under these conditions, thick macroporous membranes (>300 nm) with pore diameters exceeding 150 nm and replicating the pore structure of the underlying AAO membrane could be prepared. Similar structure was obtained with cobalt films on AAO by using PLD in a high-energy mode.[19] At low kinetic energy conditions (e.g., below a few mbar of helium), a continuous film is rapidly formed and the characteristic structure of the AAO membrane is not discernable. The SEM image is thus a flat grey image and thus not presented. In that case, the film properties are similar to those obtained for films deposited on conventional flat substrates under the same conditions. With increasing background pressure, multiple collisions between the plume species and the background gas molecules induce a plume confinement and therefore a decrease in the velocity of the ablated species. In that regime, diffusion at the surface of the substrate is significantly reduced and hence the formation of porous, textured and polycrystalline films is observed. A study correlating gold film structure and morphology with plasma expansion parameters (i.e kinetic energy of the species) was reported by Irissou et al..[20] The Au films were thus deposited under two distinct deposition conditions by changing both the background pressure and the target to substrate distance ($d_{t\text{-}s}$ = 4 cm and 2 cm under vacuum and 3 mbar of helium, respectively).

Figure 2 shows the effect of the deposition atmosphere on the gold film. When deposited under vacuum, we clearly observed the porosity of the substrate and the film appears black. When deposited under helium atmosphere, the nanoparticles fill the pores at the surface, which appears more or less flat with some roughness. The film appears as a gold-yellow colored mirror. Lu_2O_3:Eu^{3+} was then deposited onto the gold layer under oxygen atmosphere (10^{-3} mbar) allowing the morphology of the underlying layer to be retain. All deposited multilayers were then subject to rapid thermal annealing for 10 seconds at 450 °C in air. Such thermal treatment has been optimized in order to improve the crystallization state of Lu_2O_3 without damaging the AAO membrane. Indeed, this best crystallization state is favorable to enhance scintillation

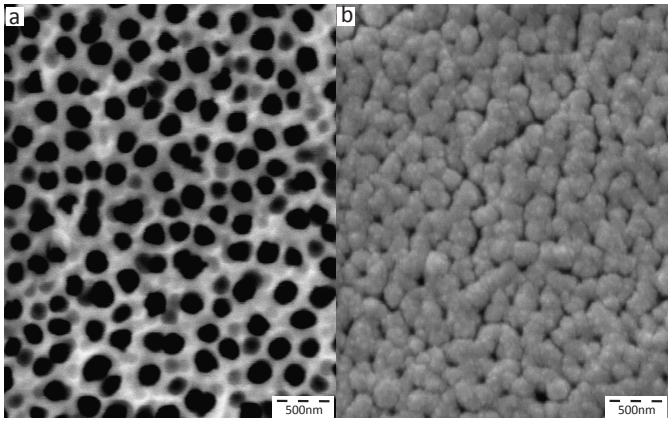

Fig. 2 Scanning Electron Microscope images at 10 kV for (a) a membrane covered with gold under vacuum (b) a membrane covered with gold under 3 mbar of helium

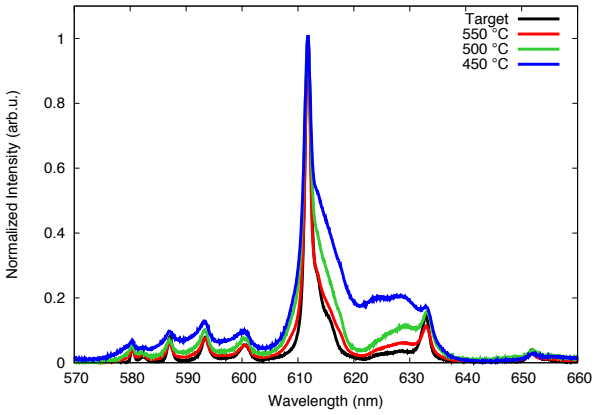

Fig. 3 Luminescence sprectra under 250 nm light excitation of (black) the target corresponding to the polycrystalline pellet, and after a rapid thermal annealing at (blue) 450 °C, (green) 500 °C and (red) 550 °C

yields since it decreases the number of non radiative trapping centers. The evolution of the crystallization state was checked with the luminescence spectra depicted in Fig. 3, and showing the narrowing of the Eu^{3+} ions emission line as a function of the temperature treatment and as compared to the crystalline target. To control the crystallization of Lu_2O_3 thin films, X-ray diffraction characterization was performed after annealing on Lu_2O_3:Eu^{3+}(450nm) / Au(5nm) thin film deposited on Al_2O_3 membrane (Fig. 4). The diffractogramm shows only one series of diffraction peaks located at 20.98° (211), 29.82° (222), 34.58° (400), 44.53° (134), 49.66° (440) and 58.96° (622).This agrees well with the peak positions expected for Lu_2O_3 (JCPDS-ICCD card #00-043-1021). The peak positions do not shift toward larger 2θ values by more than 0.09°, indicating that the structure of the Lu_2O_3 matrix is not modified by the doping with europium (1%). The deduced lattice parameter a_{hkl} obtained from the main diffraction peaks is 1.0383 nm, which corresponds well to the value found in the literature (JCPDS-ICCD card #00-043-1021). Finally, Fig. 1 shows that the final multilayer component composed of the substrate, 20 nm of gold and 450 nm of scintillator exhibits an X-ray attenuation in good agreement with the theoretical calculation (orange line and full triangles).

3.3 Imaging performances

In order to evaluate the imaging performances of the multilayer screen, radiographic images of a tungsten pattern with various lines separations were performed. The reference screen made of 250 μm thick $Y_3Al_5O_{12}$:Ce^{3+} (YAG) currently used for beam diagnosis and which corresponds to the state of the art was measured in the same conditions (called reference screen). Note that this screen is probably the best system for high-resolution imaging but is note suitable for online beam diagnosis because its 250 μm thickness exhibits a weak transparency of the X-ray beam. The obtained results are presented in Fig. 5. When Lu_2O_3:Eu^{3+} is directly deposited on the porous AAO substrate, the luminosity is sufficient to obtain an image, but it can be seen on Fig. 5 that the image is not sharp, as it is observed with the reference screen. The effect is attributed to the contribution of the reflected/diffused image at the interface with the porous substrate which contributes to a blurring effect. In order to suppress this contribution, a gold layer was interposed. When prepared under vacuum, the layer appeared black due to gold covering the substrate while preserving the porosity. The direct impact can be seen in Fig. 5 where details down to few μm are now observed with the pattern. Table 1 resumes the Contrast Transfer Function (CTF) deduced from these images. One may remark that the imaging capability are competing with the reference screen, with a luminosity reduced by a factor of 80 due to the weaker thickness of active material (450 nm against 250 μm). This screen can be improved even more when the gold deposition is performed under weak helium pressure. As explained above, such a deposition condition enables the porosity with gold nanoparticle to vanish. The surface substrate acts as a mirror, and reflected light contributes in a positive manner to the image regarding resolution. The detected luminosity is about twice those detected with the previous screen, and even more interestingly the image quality is slightly improved. As a comparison, we performed a radiographic image of a piece of foam (Fig. 6-left part) and the image is clearly more detailed when gold is deposited under helium pressure.

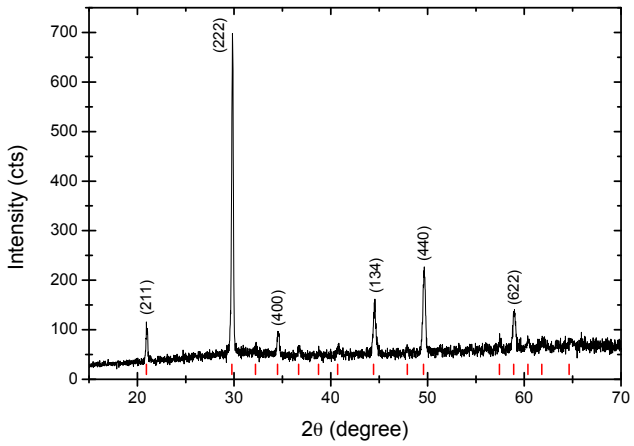

Fig. 4 X-ray diffraction pattern of annealed Lu_2O_3:Eu^{3+} (450nm) deposited on the Al_2O_3 membrane and including a Au(5nm) thin film as interposer. Red ticks indicate the peak positions of Lu_2O_3 according to the JCPDS-ICCD card #00-043-1021

In order to quantify the image capability, Modulation Transfer Function (MTF) has been deduced from a radiographic image of a tungsten edge (Fig. 6 right). The effect of gold interposer can be clearly seen since the MTF approaches the diffraction limit in/Users/christophe.dujardin/Desktop/dossier sans titre the case of a multilayer screen containing gold deposited under He pressure and 450 nm Lu_2O_3:Eu^{3+} scintillating layer.

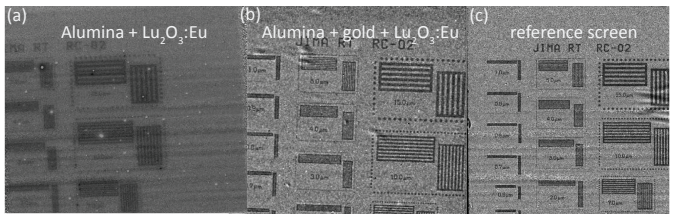

Fig. 5 Uncorrected radiographic images of a pattern performed at 15 keV with Lu_2O_3:Eu^{3+} scintillating film directly deposited on the substrate (a) and with an intermediate gold buffer prepared under vacuum (b). For illustration (c) is the image obtained with an absorbing screen generally used for beam diagnostic (250 μm thick $Y_3Al_5O_{12}$:Ce^{3+}). The 1 μm thick tungsten micro-chart exhibits patterns from 15 μm down to 0.4 μm with 16 different widths.

3.4 Online X-ray beam analysis capability

In the previous sections, it has been demonstrated that the proposed screen weakly absorbs X-rays (for energies above 10 keV) and provide very good imaging capability. The beam analysis consists in receiving the position and shape of the incident beam as fast as possible in order to propose an online

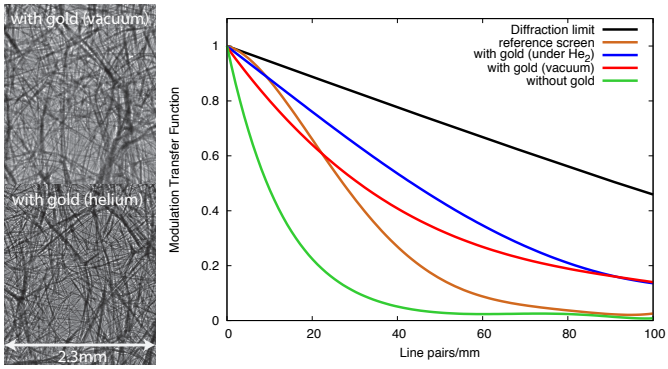

Fig. 6 Left: Uncorrected radiographic images of a piece of foam performed with Lu_2O_3:Eu^{3+} scintillating film deposited on the substrate with an intermediate gold buffer deposited under vacuum and under 3 mBar He pressure. Right: Modulation Transfer Function (MTF) deduced from the image of an edge for the reference screen made of thick Y_3AlO_5:Ce^{3+} (orange), a Lu_2O_3:Eu^{3+} scintillating film directly deposited on the substrate (green), Lu_2O_3:Eu^{3+} scintillating and an intermediate gold buffer deposited under vacuum (red) and under He pressure (blue). Dark: theoretical MTF based on the diffraction limit.

Table 1 Contrast transfer function (CTF) deduced from the radiographic images of the pattern obtained in Fig. 5. The CTF is defined as $(I_{max} - I_{min})/(I_{max} + I_{min})$, where I_{max} and I_{min} are the maximum and minimum intensities detected along the on series of line of the various patterns (line separation 15,10 and 5 μm)

	Lu_2O_3	Lu_2O_3/Au	YAG
15 μm	0.057	0.171	0.0146
10 μm	0.045	0.180	0.141
5 μm	-	0.093	0.109

correction. We performed images of a focused X-ray beam at rather low intensity (2 10^{10} ph/sec in the spot) as compared to modern X-ray beamlines which propose X-rays fluxes two orders of magnitude higher and at 10 keV. Beam shape has been recorded with 50 ms integration time using an optical magnification of the image leading to a pixel size of 3.75 μm. Gaussian fitting enables the reconstruction of the X-ray beam profile, exhibiting in this case different widths along two selected directions: $\sigma_x = 4.99$ μm and $\sigma_y = 6.64$ μm respectively (Fig. 7). In alignment-only procedures, beam shape correction is used and only fluctuations of position and intensity are required during experiments. Instead of using a fitting procedure which is time-consuming over many images, position of the image barycenter is computed online. We tested this technique with the worst beam profile shape, namely a spot having a dimension of 11 μm FWHM. We thus moved the beam step by step and so easily detected these displacements down to 500 nm with a spread of positioning with a variance

of σ_x = 50 nm and σ_y = 146 nm.

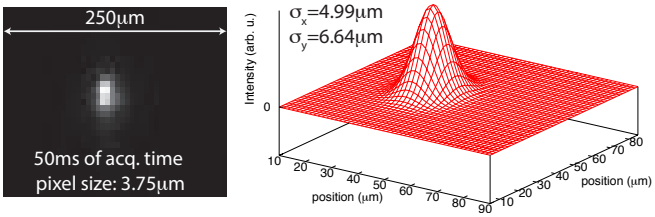

Fig. 7 (Left: 10 keV X-ray focused beam image during an acquisition time of 50 ms. (X-ray flux of 2.10^{10} ph/sec in the spot). Right: deduced beam profile using Gaussian function fitting (R^2 = 0.98 along both directions)

4 Conclusions

In this contribution, we demonstrate that nanometric scintillating layers made of Lu_2O_3:Eu^{3+}, deposited using Pulsed Laser Deposition on a porous alumina substrate, is suitable for online X-ray beam analysis in terms of X-ray transparency. When a gold nano layer is interposed as nanoparticles, it even significantly improves the imaging capability and renders the multilayer screen completely functional. Several similar screens have been now prepared and will be installed on several beamlines for evaluation in various conditions at the European Synchrotron Radiation Facility (flux, energy, long acquisitions).

References

1 G. Martinez-Criado, R. Tucoulou, P. Cloetens, P. Bleuet, S. Bohic, I.Kieffer, E. Kosior, S. Labouré, S. Petitgirard, A. Rack, J. A. Sans, J. Seugura-Ruiz, H. Suhonen, J. Susini and J. Villanova, *J. Sync. Radiat.*, 2012, **19**, 10–18.

2 S. Kelly, J. Trenkle, L. Koerner, S. Barron, N. Walker, P. Pouliquen, M. Tate, S. Gruner, E. Dufresne, T. Weihs and T. Hufnagel, *J. Sync. Radiat.*, 2011, **18**, 464–474.

3 M. Fuchs, K. Holldack, G. Reichardt and U. Mueller, Synchrotron Radiation Instrumentation, Pts 1 and 2, 2007, pp. 1006–1009.

4 R. van Silfhout, A. Kachatkou, N. Kyele, P. Scott, T. Martin and S. Nikitenko, *Opt. Lett.*, 2011, **36**, 570–572.

5 B. Solar, H. Graafsma, J. Morse, M. Salomé, G. Potdevin and U. Trunk, SRI 2009: The 10TH International Conference on Synchrotron Radiation Instrumentation, 2010, pp. 846–850.

6 A. Koch, C. Raven, P. Spanne and A. Snigirev, *J. Opt. Soc. Am.*, 1998, **15**, 1940.

7 D. Lowndes, D. Goehegan, A. Puretzky, D. Norton and C. Rouleau, *Science*, 1996, **272**, year.

8 M. Ashfold, F. Claeyssens, G. Fuge and S. Henley, *Chem. Soc. Rev.*, 2004, **33**, 23.

9 H. Christen and G. Eres, *J. Phys.-Condens. Mat.*, 2008, **20**, 264005.

10 A. Lempicki, C. Brecher, P. Szupryczynski, H. Lingertat, V. V. Nagarkar, S. V. Tipnis and S. R. Miller, *Nucl. Instrum. Meth. A*, 2002, **488**, 579.

11 T. Martin, P. A. Douissard, Z. Seeley, N. Cherepy, S. Payne, E. Mathieu and J. Schuladen, *IEEE T. Nucl. Sci.*, 2012, **59**, 2269.

12 Z. Marton, H. B. Bhandari, C. Brecher, S. R. Miller, B. Singh and V. V. Nagarkar, *IEEE T. Nucl. Sci.*, 2013, **60**, 983.

13 V. V. Nagarkar, S. R. Miller, S. V. Tipnis, A. Lempicki, C. Brecher and H. Lingertat, *Nucl. Instrum. Meth. B*, 2004, **213**, 250.

14 C. Martinet, A. Pillonnet, A. Lancok and C. Garapon, *J. Lumin.*, 2007, **126**, 807.

15 A. Garcia-Murillo, C. L. Luyer, C. Dujardin, T. Martin, C. Garapon, C. Pedrini and J. Mugnier, *Nucl. Instrum. Meth. A*, 2002, **486**, 181.

16 E. Zych, M. Wawrzyniak, A. Kossek, J. Trojan-Piegza and L. Kepinski, *J Alloy Compd.*, 2008, **451**, 591.

17 C. Dujardin, D. Amans, A. Belsky, F. Chaput, G. Ledoux and A. Pillonnet, *IEEE T. Nucl. Sci.*, 2010, **57**, 1348.

18 A. Pereira, F. Laplante, M. Chaker and D. Guay, *Adv. Funct. Mater.*, 2007, **17**, 443.

19 C. Jin, S. Nori, W. Wei, R. Aggarwal, D. Kumar and R. Narayan, *J. Nanosci. Nanotechno.*, 2008, **8**, 6043.

20 E.Irissou, B. Drogoff, M.Chaker, M.Trudeau and D.Guay, *J.Mater.Res.*, 2004, **19**, 950–958.

A novel multi-layered screen for X-ray beam analysis at high speed with a high imaging resolution capability. The route toward real-time beam corrections for synchrotron experiments.